Università degli Studi di Sassari

Facoltà di Medicina Veterinaria

Corso di Dottorato in Scienze Veterinarie

XXXIV Ciclo

Curriculum: Riproduzione, patologia, allevamento e benessere animale

"Strain elastography of injured equine Superficial Digital Flexor Tendons: a reliability study of manual measurements"

Tutor

Prof. Eraldo Sanna Passino

Tesi di Dottorato di Ricerca

Dott.ssa Valentina Secchi

Anno Accademico 2021-2022

Summary

Strain Elastography is an ultrasound-based technique that assesses the mechanical properties of tissues and gives a relative representation of elasticity. Early diagnosis of tendon injuries and long-term monitoring of the healing process are key to equine practice; thus, an accurate method is needed for analysing and interpreting the images obtained from injured superficial digital flexor tendons of horses.

The first aim of the study was to demonstrate the intra-operator repeatability and inter-operator reproducibility of manual measurements of elastograms obtained from injured superficial digital flexor tendons of horses; the second aim was to perform a standardization of the manual measurement method by comparing it with an external software. Despite its subjectivity, manual measurements proved to be repeatable and reproducible. In addition, the results obtained with the manual method matched those obtained with the external software.

1. Introduction

1.1 Structure and mechanic of tendons

Tendons are strong and resistant structures of fibrous connective tissue that connect muscle to bone. They are able to resist tension and high forces during muscle contraction, permitting the transmission of muscle forces to the skeletal system and then consenting joint movement.

Macroscopically, tendons are characterized by a white colour and a cylindroid or flatten shape; they constitute the extremities of body muscles and originate from the inner part of them or on their surface, where they can extend and be considered as aponeurosis. The bond between muscular fibres and tendons is called myotendinous junction, and it is permitted by the connection of muscular connective membranes with connective tissue of tendons. Finally, tendon insertion on bones is allow by superficial fibres that insert on periosteum and by deeper fibres which penetrate the bone, infiltrating and guaranteeing a firm bond.

Microscopically, tendons are predominantly composed of collagen molecules, which are organized into a multi-hierarchical structure. The main structural components are the collagen fibres, which are characterized by a wavy shape. They are composed by collagen filamentous fibrils and are arranged into fibre bundles through lax connective tissue, called endotenon. The fibre bundles are named as primary (subfascicles), secondary (fascicle) and tertiary bundles and are almost parallel to the long axis view of the tendon (Fig.1). Because of this complex and particular organization, tendons are characterized by a high tensile strength[1].

Tendon also contains a low amount of non-collagenous proteins, numerous tendinous cells, tenocytes or fibroblasts, and rare elastic fibres. Extracellular matrix is predominantly composed of proteoglicans and glicoproteins[2 3].

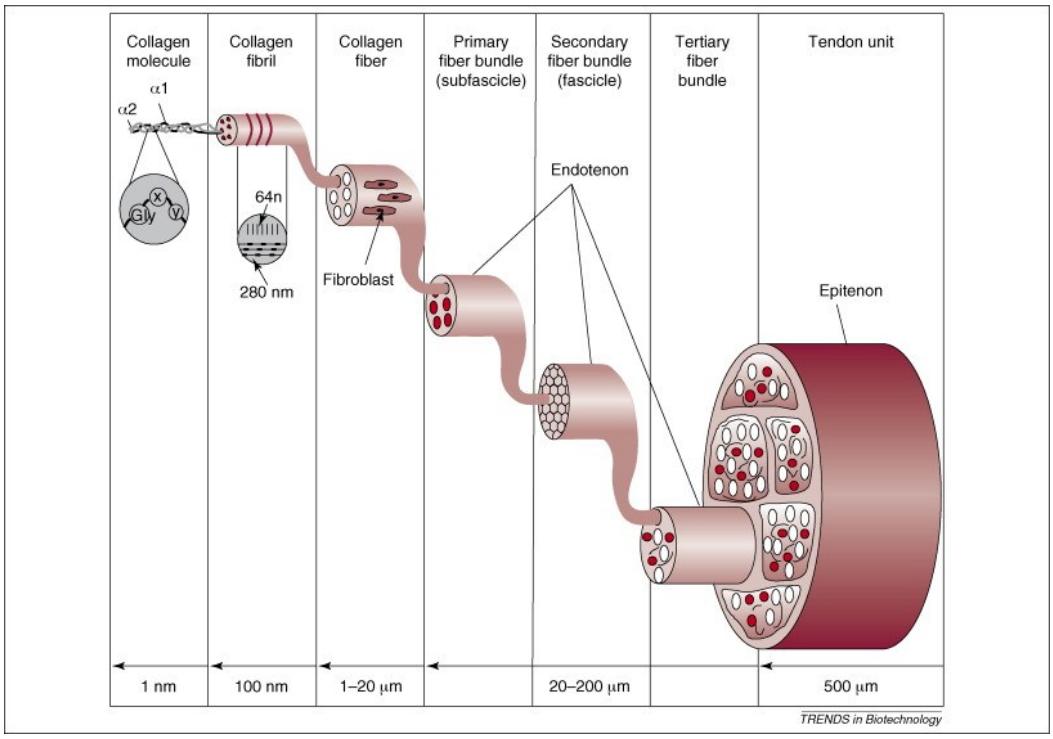

Figure 1. *From Liu et al, 2008*

Despite their great resistance to tension, their flexibility and elasticity, tendons have an inadequate extensibility. When tendons are subjected to a huge load, they do not deform linearly.

Considering the stress-strain curve (Fig. 2), the deformation (stress) of tendons caused by an external force (strain) can be divided into four phases or regions: toe, elastic, plastic, and rupture region. In the toe region collagen fibres unfurl with increased strain on tendons, experiencing very low stress. In the elastic region collagen fibres stretch with 100% of elastic recoil, so if they are stretched, they experience a stress but can return to their original shape. In the plastic region, elastic recoil reduces from the yield point to the failure point; so, collagen fibres do not return to their original length with permanent modification on tissue lengthening and comparison of small alterations (microtears). This phase can potentially precede a severe and real injury. In the final region fibres are no more subjected to stress if a strain occurs because they experience a drastic and complete rupture (tear)[43].

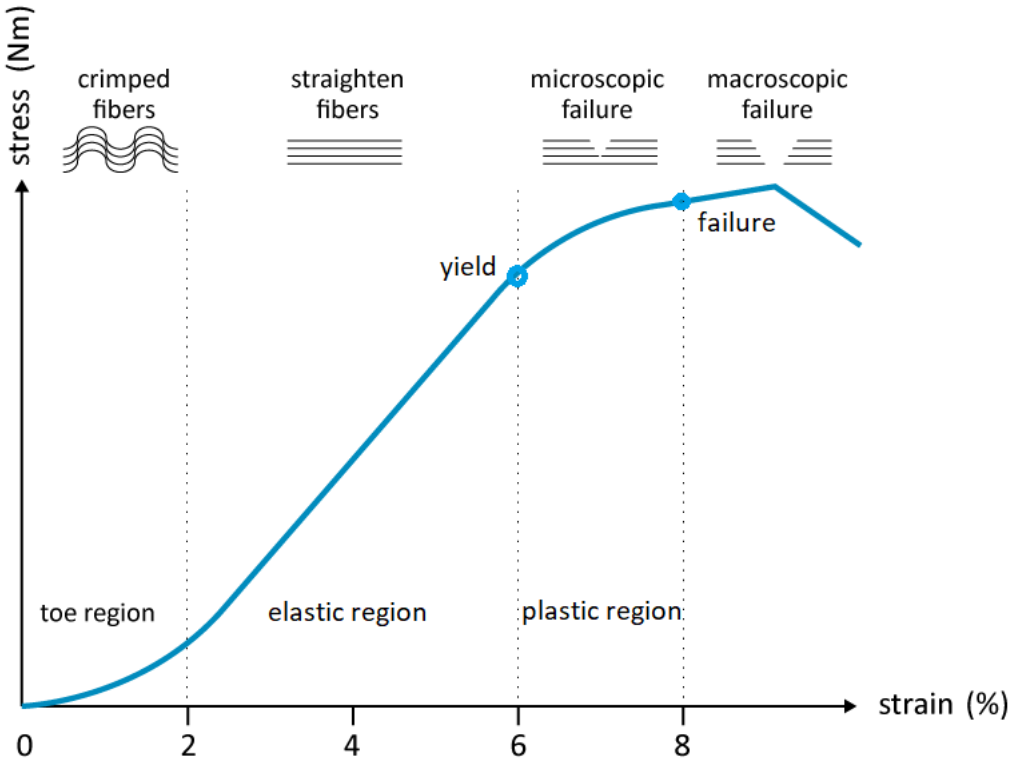

Figure 2. Stress-Strain curve. Modified from Barford, 2014.

1.1.1 Superficial and deep digital flexor tendons

The superficial digital flexor tendon (SDFT) and the deep digital flexor tendon (DDFT) are fibrous and tough structures which permit the insertion of the homonymous muscles in the distal part of each limb, at the level of the phalanxes (Fig. 3).

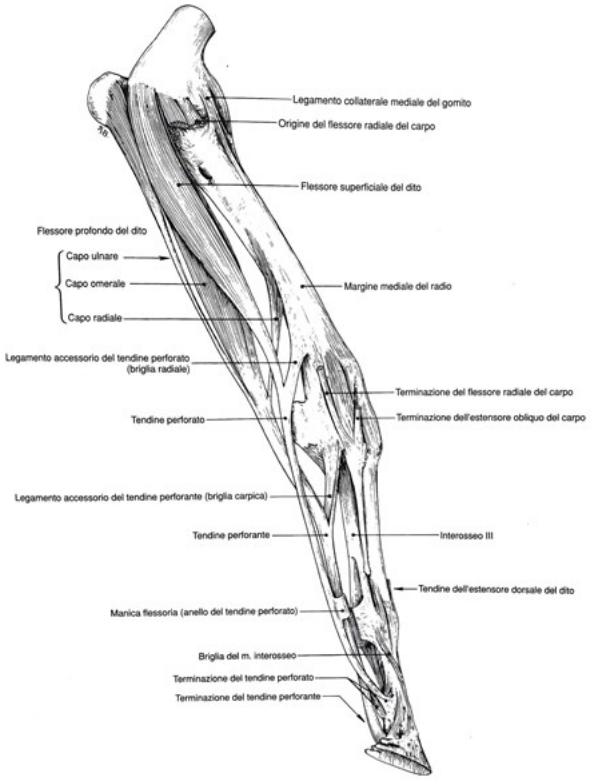

Figure 3. *From Barone, 2004*

The superficial digital flexor muscle is flat, long and prismatic; it is localized on the palmar aspect of forearm, intimately adherent to the deep digital flexor muscle. The deep digital flexor muscle is composed of three unequal parts: omeral, ulnar and radial. The omeral body is the biggest and the strongest part, with a prismatic shape; its tendon is voluminous and is unified to the thinner ulnar and radial tendons, generating a unique structure, the DDFT. Then, the DDFT goes through the carpal canal, together with the SDFT, and at the middle third of metacarpus/metatarsus it receives a strong accessory ligament, which inserts on the *carpus*.

The SDFT originates from the distal quart of forearm, receiving a strong accessory ligament, that inserts on the palmar aspect of radio. At this level SDFT is cylindric and enters in the carpal canal, near to the medial-palmar aspect of the DDFT. Here both tendons are enveloped by a common synovia.

Then, at the level of metacarpus and metatarsus, SDFT progressively flattens and appears in section as a semilunar structure, with the concavity that surrounds the DDFT, which appears progressively with an

ovoidal shape. At the level of the proximal sesamoid bones, SDFT extensions form the *manica flexoria*, in which the DDFT is enveloped.

At the level of proximal phalanx SDFT divides into two strong and short branches which insert on the glenoid *labrum*. The DDFT passes through these two branches, inserting finally on the semilunar margin of the third phalanx. In the pastoral area, inside the digital sheath, both tendons, SDFT and DDFT, are surrounded by a common synovia. It is characterized by numerous recesses, which if distended by fluids can be macroscopically evident (Fig.4).

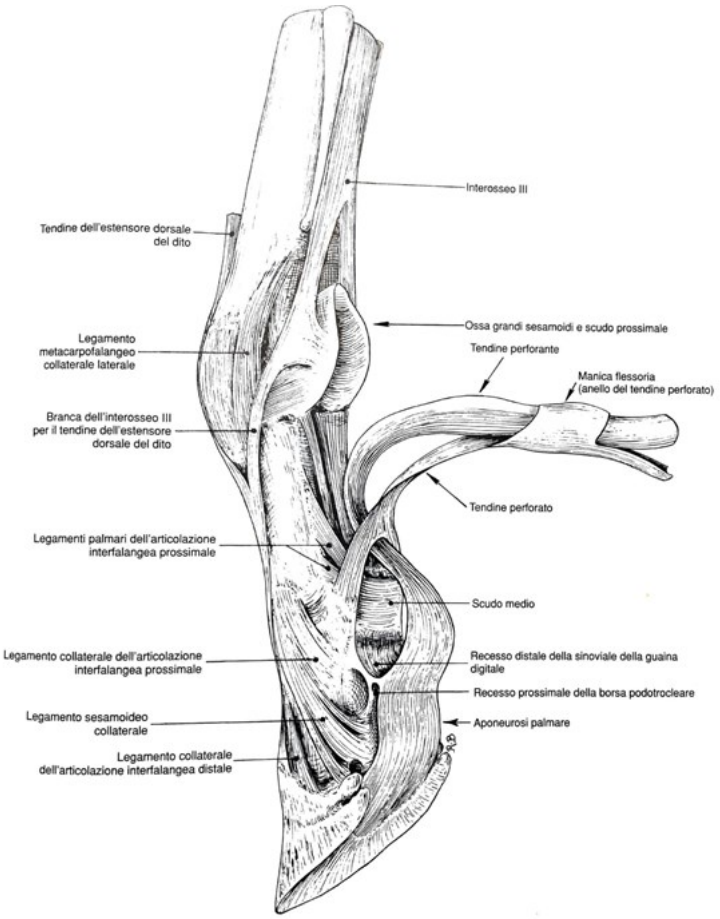

Figure 4. *From Barone, 2004*

1.1.2 Pathology of tendons

Thanks to evolution and domestic selection, the equine distal limb, with its strong and elastic ligaments and tendons, has become a valid system that led to an efficiency of movements[5].

Nevertheless, during maximal exercise the SDFT works close to its physiological limits with a thin safety margin. Considering this and a progressive degeneration that can potentially occurs when structures are stressed, clinical tendinopathy usually have an high incidence [6,7].

Tendon injury can occur after a single over strain event or for cumulative fatigue failure due to cyclical stress and overuse. In the equine SDFT, exercise and age related microdamage associated with an insufficient adaptive ability, makes fatigue failure the most likely event.

Despite the recent scientific progress, our comprehension of tendon physiological status and of the pathophysiology of SDFT injury and healing is still incomplete, as well as the effects of maturation, exercise, and training. Actually, treatment and rehabilitation of horses with SDFT injury are very difficult and the tendon requires long time for complete healing; for this reason, prevention of tendon injury could be a more feasible goal and it must become a priority.

1.2 Diagnostic Imaging techniques

Different diagnostic imaging techniques are currently available for the evaluation of tendon injury. The most commonly used are magnetic resonance imaging (MRI) and ultrasound (US).

MRI has been the gold standard for assessment of tendon lesions thanks to its excellent soft tissue contrast detail and multi-planar imaging capacities[8]. Nevertheless, it is also expensive and of limited availability.[9]

With the improvement of technologies, ultrasound modalities are being increasingly used in the evaluation of musculoskeletal system, becoming a great alternative or at least a complementary tool to MRI for the diagnosis of tendon injuries and monitoring tendon healing. The advantages that make US a reliable and more efficient method are multiplanar imaging capacity, high performance in detection and quantification of soft tissue abnormalities, being non-invasive and eventually portable, and the unique characteristic of being a dynamic imaging technique. [9–12]

1.2.1 Ultrasonography

Ultrasonography is a fundamental imaging modality for the assessment of equine soft tissues, especially in the distal limb. Diagnosis of tendon and ligament injuries is a daily practice in equine medicine, and it is performed in real time and easy way thanks to ultrasounds.

Superficial digital flexor tendon injuries are the most frequent lesions diagnosed, for this reason only metacarpal and metatarsal ultrasonography will be considered.

For the complete evaluation of the palmar aspect of soft tissue structures in the metacarpal and metatarsal regions, the most used system consists of dividing the distance between carpometacarpal joint and distal sesamoid bones into seven regions for transverse plane in the fore limb (Fig. 5) and in nine regions in the hind limb; for longitudinal scans three regions are considered for both fore and hind limbs (Fig. 6).

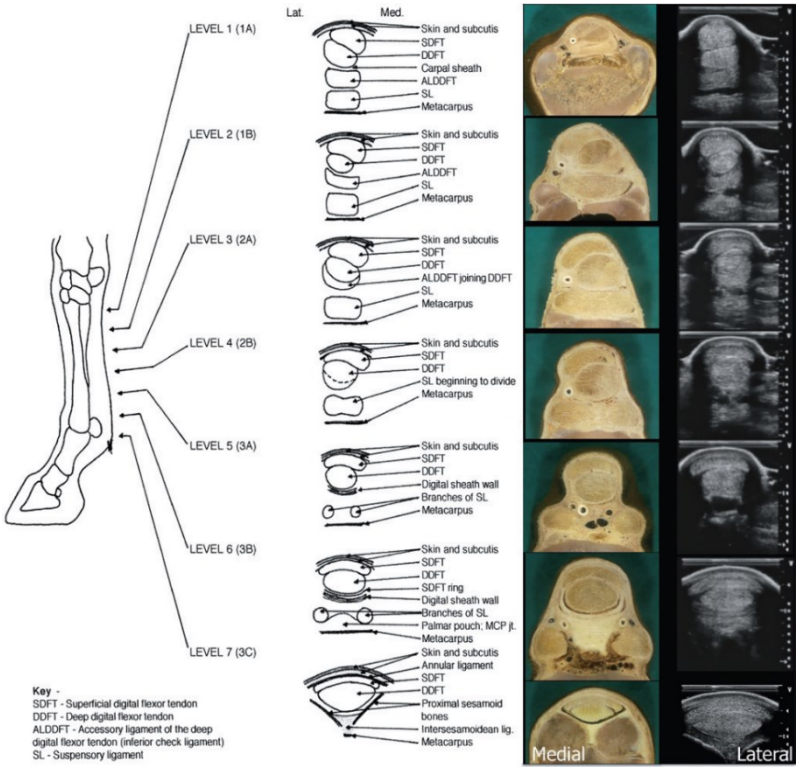

Figure 5. *From Smith and Cauin, 2014, Ultrasonography of Metacarpus and Metatarsus, Atlas of equine Ultrasonography. Normal ultrasonographic appearance of tendons and ligaments. Seven regions are considered for the transverse evaluation of palmar metacarpus area.*

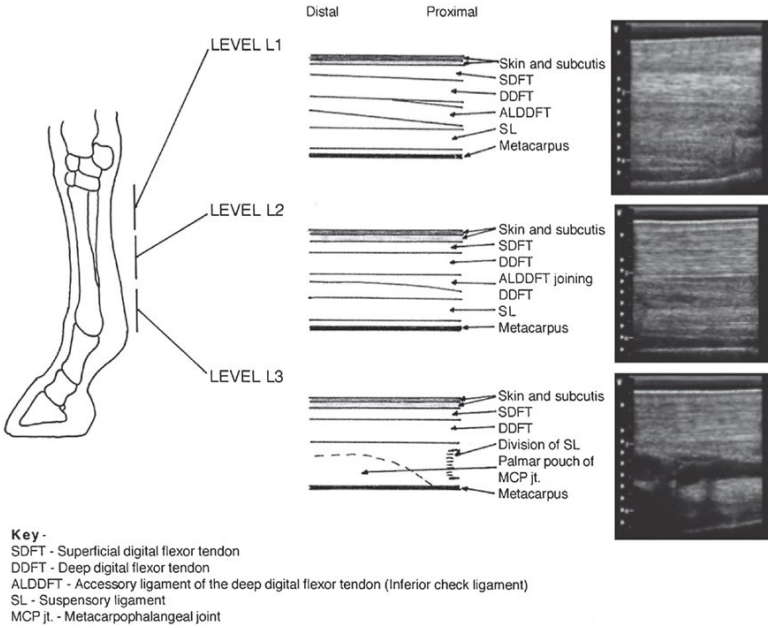

Figure 6. *From Smith and Cauin, 2014, Ultrasonography of Metacarpus and Metatarsus, Atlas of equine Ultrasonography. Normal ultrasonographic appearance of tendons and ligaments. Three regions are considered for longitudinal evaluation of palmar metacarpus area.*

An alternative ultrasonographic method consists in measuring the distance from the distal palpable margin of the accessory carpal bone or from the *tuber calcis* to the ultrasonographic section assessed. The first method is more objective but the second one could be useful for comparisons of images during follow-up in the same animal[13].

A good examination should start with a proper preparation of the animal. It should stand completely weightbearing in order to maintain ligaments and tendons under tension; nevertheless, the evaluation of the non-weightbearing limb could be useful for doppler exam and for assessment of motion of structures. Then the preparation of the skin is fundamental; it involves clipping, when possible, cleaning with water and alcohol and applying the ultrasound gel.

A high frequency (7-13 MHz) linear probe is recommended for tendons and ligaments examination, because it permits to obtain a better resolution of superficial structures. It must be held perpendicular to the examined structure to avoid artefacts, even if tilts of the probe can be useful to obtain off-incidence views and perform a more complete evaluation.

A stand-off pad is suggested to improve probe contact with skin and avoid superficial low resolution.

The evaluation of both normal and pathologic structures must be methodical, performed from proximal to distal, first in transverse then in longitudinal scan, including the measurement of cross-sectional area (CSA), the assessment of echogenicity and pattern appearance, and characterization of shape and margins.

Normal flexor tendons and ligaments of the palmar aspect of metacarpus and metatarsus appear with a fine striated pattern in longitudinal scan and with a granular appearance on transverse plane because of the presence of both collagen fibres (hyperechoic) and connective tissue interposed (hypoechoic) (Fig. 7).

Their shape especially in transverse plane differs depending on the region assessed, and margins are usually smooth and rounded. CSA depends both on the region of the tendon or ligament examined and breed and size of the horse.

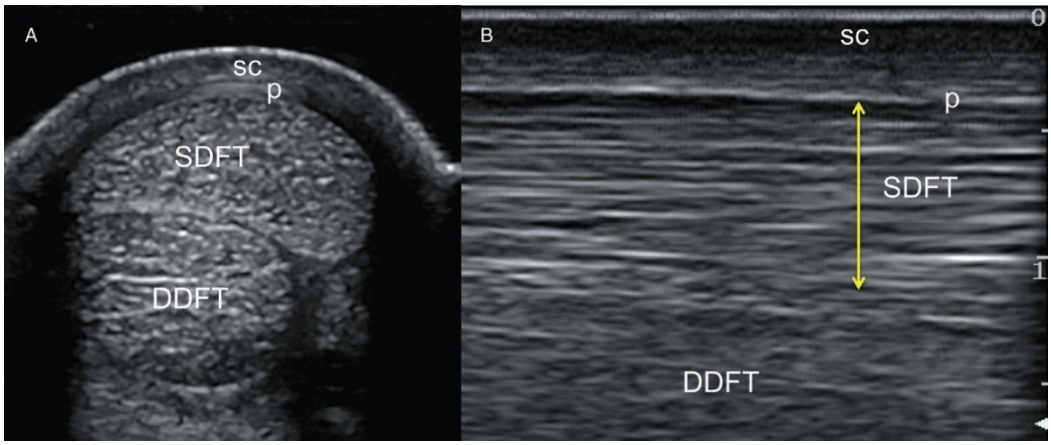

Figure 7. *From Smith and Cauin, 2014, Ultrasonography of Metacarpus and Metatarsus, Atlas of equine Ultrasonography. Example of normal ultrasonographic pattern in transverse (A) and longitudinal plane (B). SDFT (Superficial digital flexor tendon), DDFT (Deep digital flexor tendon), sc (subcoutaneous tissue), p (paratenon). Width of SDFT (yellow arrow).*

Pathologic tendons and ligament differ from their normal aspect depending on the type and severity of injury.

Acute lesions in the first few days normally appear poorly defined and heterogeneous, but a loss of the normal striated pattern and reduction in echogenicity could be visible in long-axis view. An increase in size could be associated and confirmed comparing the images with the contralateral limb.

Acute lesions, immediately after the injury, are characterized by the presence of matrix debris and clots which may have variable echogenic appearance; at this stage diagnosis of lesions could be difficult as they can have similar echogenicity compared to normal parenchyma.

Then, after few days, as the water content rises, because of oedema, and immature granulation tissue forms, tendon or ligament lesions have a decreased echogenicity and become more evident. Even peritendinous or subcutaneous tissue could be affected and appear more hypoechoic with an evident thickening.

Considering the SDFT, a common manifestation of acute injury is the well-known “core lesion” (Fig. 8), an area of evident hypoechogenic appearance visible in the centre of the tendon, even though they could also be more eccentrical. It usually affects the mid-metacarpal region. A concomitant increase in CSA is commonly present.

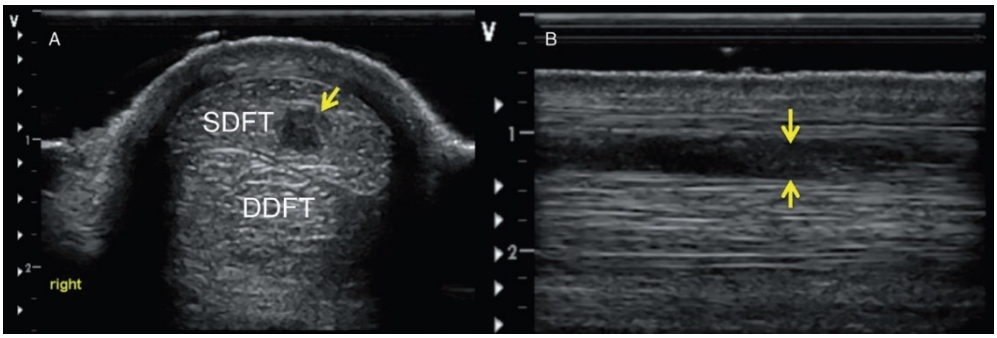

Figure 8. *From Smith and Cauin, 2014, Ultrasonography of Metacarpus and Metatarsus, Atlas of equine Ultrasonography. Example of core lesion (yellow arrows) in transverse plane (A), and longitudinal plane (B) with loss of striated pattern.*

In order to measure the total size of a lesion, both the CSA and the proximo-distal extension of the injury must be evaluated. This is useful to obtain a semi-objective assessment of severity and establish a correct prognosis for the animal. In particular, the percentage ratio of damaged tendon can be calculated by comparing the CSA of tendon lesion with the total tendon CSA at each level for all seven regions in transverse scan. An approximation of the volume ratio of the lesion for the total tendon is obtained (Fig. 9). Injuries are considered mild if the ratio is 0-15%, moderate for 16-25% and severe if >25% [13].

Diffuse lesions are also possible, even if more challenging to diagnose. The long-axis loss of striation helps for the assessment.

A complete rupture of SDFT is the most severe eventuality, with a complete loss of striation and an evident anechoic area present between the two fragments of the ruptured tendon and surrounded by a thin hyperechoic line (paratenon).

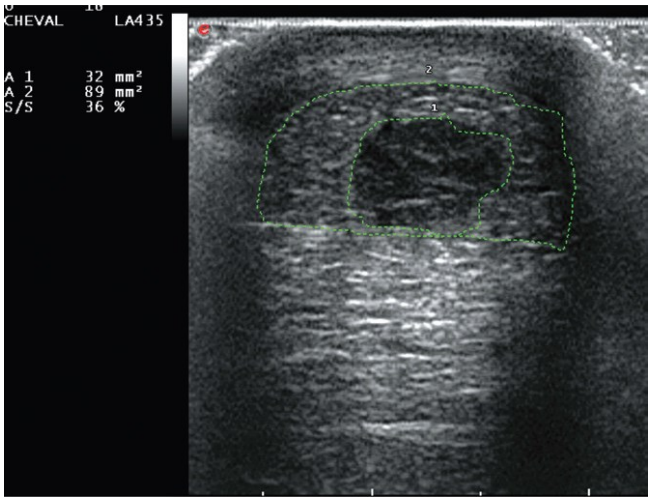

Figure 9. *From Smith and Cauin, 2014, Ultrasonography of Metacarpus and Metatarsus, Atlas of equine Ultrasonography. Example of volume ratio of the lesion. Ratio > 25% = severe lesion.*

1.2.2 Ultrasound Elastography

Introduced in the early 1990s by Dr. Jonathan Ophir [14], Elastography, abbreviation for Ultrasound Elastography, also referred to as Elasticity Imaging (EI), is a relatively new diagnostic imaging technique which shows elasticity pattern of tissues instead of their morphology. This ultrasound-based method allows the qualitative visualization or quantitative measurements of the mechanical properties of tissue, providing information on tissue stiffness. It complements the information produced by conventional B-mode and Doppler-imaging, expanding the frontiers of diagnostic imaging [14–18].

For centuries elastic properties of tissues have been evaluated with palpation, which was the unique method able to evaluate the consistence of lesions and to discriminate the eventual malignity of them, in case of neoplasia. Elastography then could be considered as an alternative method, able to substitute the physical clinical exam or at least to be associated with.

The main principle of the system consists in the application of a force (stress) on the tissues generating a displacement of them, which correlates with the elasticity properties.

Over the years, many techniques have been developed, with differences regarding the type and intensity of force applied and the method used for processing and displaying the relative images of elasticity pattern.

Actually, the main existing methodologies are Acoustic Radiation Force Impulse Imaging (ARFI), Shear Wave Elastography (SWE), Supersonic Shear Imaging (SSI) and Strain Elastography (SE).

Acoustic Radiation Force Impulse Imaging (ARFI) (Fig. 10) creates a qualitative 2-D map of elasticity or shows a quantitative value (wave velocity value expressed in m/s) of tissue stiffness performing a compression inside the tissue using the acoustic radiation force from a focused ultrasound beam. The displacement of the tissue in a selected region along the axis of the ultrasound beam depends on the compressive force applied and reflects the grade of elasticity of the tissue[19].

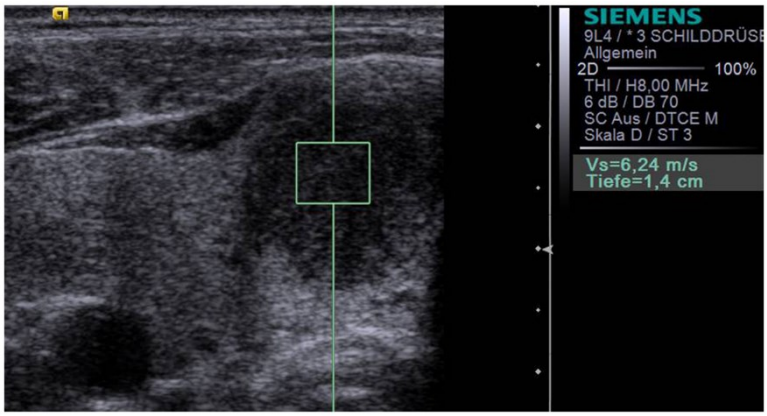

Figure 10. *From Bojunga et al (2012). Example of rapresentation of ARFI technique.*

Shear Wave Elastography (Fig. 11) is a technique that permits to determine the elastic properties applying an ultrasound impulse on the tissues. This impulse generates transversal waves (shear waves) perpendicular to the direction of ultrasounds.

The main principle of the method is calculating the speed of shear waves using the B-mode ultrasound, which monitors the displacement of tissues generated by shear waves. Using speed values, it is possible to calculate the elasticity module of tissues. Shear waves propagate faster in harder tissues, so their speed is directly correlated to tissues stiffness. Tissue stiffness can be visualized as shear waves speed,

expressed in m/s, or more commonly it is expressed as a pressure unit, kilopascals (kPa), calculating the Young's modulus [20–23].

SWE is then able to obtain a quantitative value of tissues elasticity, representing an objective and reliable technique[24].

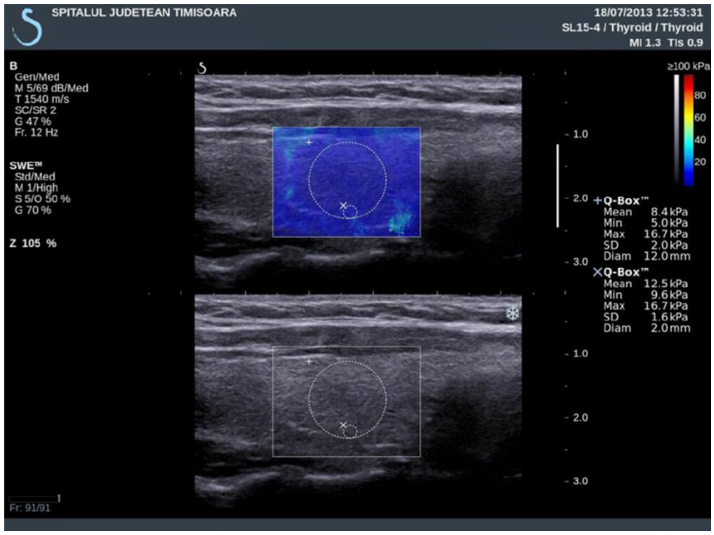

Figure 11. *From Vlad et al (2015). Example of SWE*

Supersonic Shear Imaging (SSI) (Fig. 12) is a technique that permits to obtain a quantitative real-time two-dimensional of tissue elasticity. Based on the principles of SWE, an impulse is generated from the ultrasound beam that generates shear waves propagating perpendicularly to the axis of the probe. Then, tissue elasticity is calculated and mapped considering the velocity of propagation of shear wave through the tissue [25].

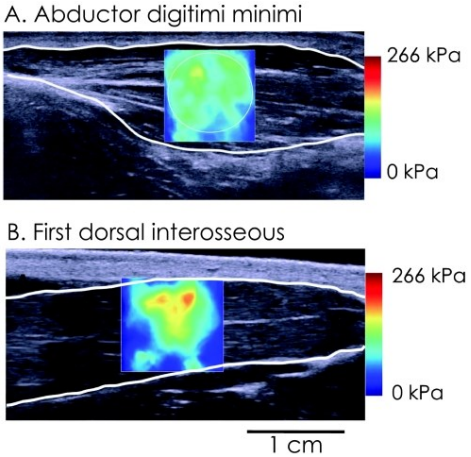

Figure 12. *From Bouillard et al (2011). Example of quantitative map elasticity obtained with Supersonic Shear Imaging.*

Strain Elastography is based on the main principle that applying a compressive force (stress) on a tissue, an axial displacement (strain) is generated [17]. The force could derive from a manual rhythmic movement applied with an hand-held transducer [10,26–31], or it could derive from physiologic body movements (respiration, pulsation) [23]. The displacement is calculated by comparing the ultrasound images before and after compression [14], obtaining a relative grade of deformability (elasticity) of the tissue within the field of view (Fov). The relative elasticity is displayed as a coloured-coded map, called elastogram, superimposed on the grey scale ultrasound image. For the elastogram, different patterns are available, from grey scale to different colour coded, depending on preference, but commonly red denotes softest tissues, blue encodes hard consistency, and green and yellow indicate intermediate stiffness [9,21,22].

The greater the grade of displacement of tissue is, the greater its elasticity and lower its rigidity. Nevertheless, it is not possible to calculate the absolute value of displacement of tissues and consequently the elastic modulus because the real value of the force applied is not measurable. For this reason and considering also factors as different levels of pressure applied, correct transducer alignment and out-of-plane movements of the probe, SE is considered a subjective and highly operator dependent technique [28].

However, the accuracy of elastography is confirmed by a visual indicator present on the side of the screen; its colour changed from grey to green when a correct compression is applied (Fig. 13).

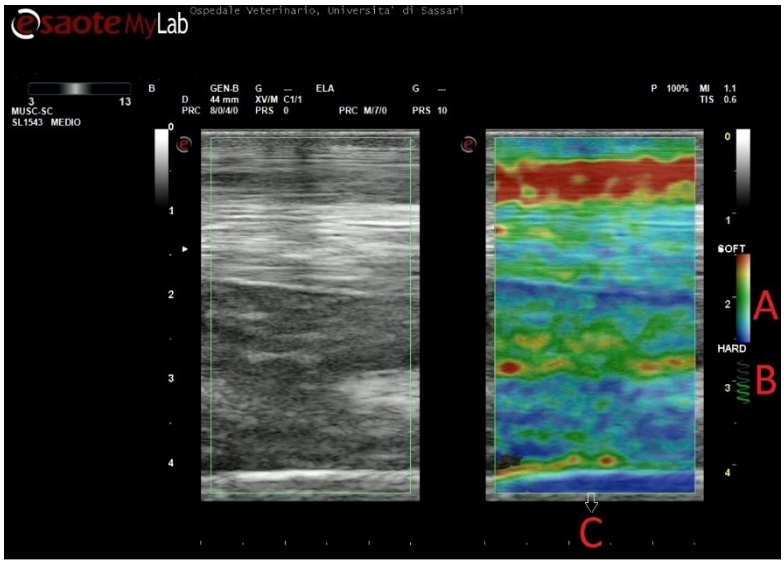

Figure 13. From Secchi et al (2021). Example of elastogram of a metacarpal region. Range of colours (A), indicator for correct compression (B), Field of view-Fov (C).

Another issue is the analysis of images and classification of lesions recognized in the Elastograms. The simpler and more famous method, used especially for classification of breast lesions in oncology, is the Tsukuba score (Fig. 14).

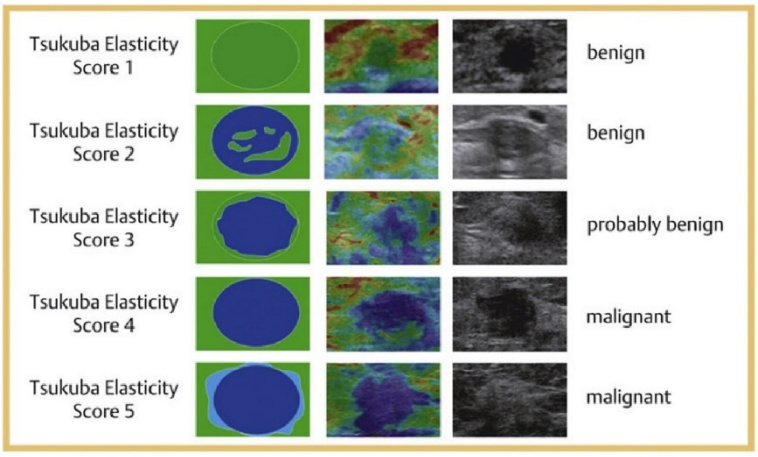

Figure 14. *From Schwab et al (2016). Tsukuba Elasticity Score*

It is characterized by a visual classification of lesions based on the prevalence of colours inside the region of interest. For this reason, it is considered a very subjective technique even if easily appliable [32].

However, semi-quantitative methods can be utilized as more objective, such as the strain ratio (Fig. 15), which shows the relative elasticity between a selected region of interest (ROI) in a tissue and a reference ROI, usually adjacent subcutaneous tissues[22,33], like for example subcutaneous fat for the evaluation of breast masses.

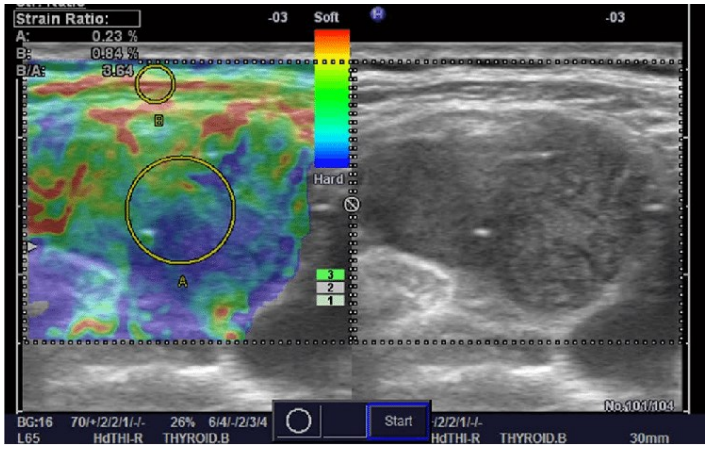

Figure 15. *From Choi et al (2015). Example of strain ratio between a metastatic linph node and a normal muscle.*

1.2.3 Elastography in Human Medicine

During the last decades, USE proved to be a useful technique in many studies for the diagnosis of different pathologies, used alone or more often as a complementary technique of other imaging modalities, like ultrasound (US) or magnetic resonance imaging (MRI).

Using conventional US, it is sometimes difficult to properly evaluate organs and differentiating between normal and pathologic tissues, due to the presence of lesions with the same echogenicity of surrounding healthy tissues.

Lesions could have different stiffness depending on the process present. Inflammation and tumours, because of their histologic characteristics, lead to changes in the normal mechanical and elastic properties of tissues. Obviously, lesions containing fluids, like in acute inflammatory response, or fat are softer than lesions with fibrotic tissue or calcifications.

In the past, in many clinical conditions, physical examination and especially palpation were the basic modalities to assess tissue stiffness, recognize eventual lesions and monitor the healing as well.
With its capacity to evaluate tissue stiffness, USE increased its importance in human medicine and became an alternative method for lesions assessment, increasing the diagnostic power of US.

USE can investigate pathologies in a wide variety of medical fields. Currently, USE is successfully applied for the assessment of breast[34], thyroid[35], liver[35] and prostatic[36] lesions by measuring tissue stiffness. In addition, it has been applied to lymph node characterization[36]. In oncology, it could be very helpful for the differentiation of benign from malignant lesions, as a greater rigidity is more likely associated to malignant diseases[37]. Then, USE could represent an alternative method for biopsy, considering also that it is safe and non- invasive[38].

Moreover, in the last few years, studies relating the use of USE in the musculoskeletal system have risen extensively, giving fundamental information regarding biomechanical properties of normal and pathologic tissues, especially tendons and ligaments[39]. Articles relating the value of USE and its application

on musculoskeletal system include studies on healthy and degenerative Achille's tendon[26,27,40], lateral epicondylitis[31], several rheumatologic conditions[41,42], and, more recently, plantar fascia[43].

The potential power of elastography in the evaluation of musculoskeletal system could be:

- Early diagnosis of degenerative tendon lesions, before clinical signs occur, in order to avoid potential worse injuries
- Diagnosis of muscular contracture in case of normal B-mode images but with the presence of clinical symptoms
- Monitoring the evolution of muscular scares and the healing of tendon injuries, in order to better plan the return to training or competing, especially in case of professional athletes.

1.2.4 Application of ultrasound elastography in Veterinary Medicine

Ultrasound elastography started recently to be utilized in veterinary medicine, and only after its application in human medicine.

Several studies have been performed on small animals, especially dogs, regarding the assessment of thyroid[44], spleen[45], lymph nodes[46,47], and prostate lesions[48,49], as well as skin and mammary masses[50–53].

A small research has been made on musculoskeletal system too, focusing on normal common calcaneal tendon[54], gastrocnemius tendon[55] and patellar ligament[56].

Regarding musculoskeletal system in equine medicine, both *in vitro* and *in vivo* articles have been published, with particular attention on normal and pathologic superficial digital flexor tendons (SDFTs)[57–62].

Despite the presence of a limited number of studies and often the few cases reported in articles, both SWE and SE, which however represents the most used technique, proved to be repeatable and reproducible methods for the assessment of different organs and structures, both normal and pathologic.

1.3 Aim of the study

Images interpretation is a fundamental step to make accurate diagnosis of equine tendon injuries and establish correct prognosis. Consequently, it is of extremely importance in order to decide and organize a proper rehabilitation of horse athletes

Considering this and the fact that the main interpretation systems for elastograms obtained with Strain elastography are incredibly subjective a more objective method is required.

In this study the method utilized for the analysis of elastograms was the manual measurement of the tendon damaged areas (mainly red) and the sound parts (mainly green and blue) compared to the total surface area of the tendon. This system, despite operator-dependent, showed quantitative values of the injured areas. So, the first aim of the study was to demonstrate the intra-operator repeatability and inter-operator reproducibility of manual measurements of elastograms obtained from injured superficial digital flexor tendons of horses.

The evaluation of images with an external software is an objective method and could represent a valid alternative for image analysis, nevertheless it is too complex to be used on a daily clinical practice and especially in the field; on the contrary, the manual method proposed in the study is more feasible. Then, the second aim was to perform a standardization of the manual measurement method by comparing it with an external software, in order to validate it and consider it as accurate as the software method.

2. Materials and Methods

2.1 Horses and preparation

Twenty Anglo-Arabian racehorses (11 mares and 9 geldings, aged between 4-9 years) with a forelimb SDFT core lesion, which had occurred during racing or training, were included in the study. Each horse was first given a clinical evaluation, and then assessed with both 2D-US and SE within two weeks from the onset of injury.

Before performing the ultrasonographic examination, the hair was cut on the palmar metacarpus, which was then washed thoroughly with water. A coupling gel was finally applied in order to improve probe contact and obtain a better resolution.

Horses were not sedated because they were all sufficiently calm.

The study was approved by the ethics committee (O.P.B.S.A.) of the University of Sassari (protocol code n° 128528, approved on 15 November 2019).

2.2 Ultrasound technique and devices

Ultrasonographic examinations were performed by one veterinarian (VS) using an ultrasound unit (My Lab Alpha, Esaote, Florence, Italy) equipped with the SE software "ElaXto" and a linear 3-13 MHz transducer.

Horses were evaluated in a square stance, under weight-bearing conditions, and forelimbs were assessed from the carpometacarpal joint to the distal sesamoid bones, dividing the palmar aspect of the metacarpus into seven levels (1-7) for transverse planes, and into three levels (1-3) for longitudinal planes. This system differentiates the metacarpal regions according to specific anatomic features, and was essential for a better comparison of the images of the various horses involved in the study [13].

The examinations were performed from proximal to distal, first in transverse then in longitudinal planes, at each level of the metacarpus. The probe was positioned in order to obtain lateral structures on the left and medial structures on the right side of the screen, in transverse orientation, and distal parts on the left and proximal parts on the right, in longitudinal orientation.

In order to obtain correct 2D-US images and to avoid anisotropy artefacts, the transducer was held perpendicularly to the surface analysed, [63]. A standoff pad was also used for the 2D-US examinations.

In the trials, power (100%), frequency (intermediate), number and position of focus, and depth (~4cm) were maintained stable.

2.3 Elastographic Evaluation

Strain elastography was performed by the same trained veterinarian (VS) applying a gentle manual rhythmic pressure with the linear transducer. As recommended by the manufacturer, the manual compression was minimal, i.e. a vibration with a movement equal or less than 1 mm [23]. A standoff pad was not used in the SE examination.

A colour-coded map was selected, with a range of red (softer tissues) through yellow/green (intermediate stiffness) to blue (stiffer tissues) colours.

A wide Fov was set and kept constant (depth of ~4cm) to obtain as detailed a chromatic scale as possible [23]. In these experimental trials, the Fov included SDFT, deep digital flexor tendon, accessory ligament of deep digital flexor tendon, suspensory ligament, and palmar border of the cannon bone.

A 2D-US image was placed simultaneously beside the elastogram to ensure that the image was maintained constant and the probe was not moved laterally, and to assess the movement of tissue during compression-release cycles (1 mm maximum). A minimal precompression was applied.

The accuracy of the elastograms obtained was evaluated during the examination by checking a visual indicator. As the correct compression was applied, the indicator colour changed from grey to green, and a videotape was recorded for each level of the metacarpus (Fig. 16).

Only images in long-axis view were selected for the following analysis.

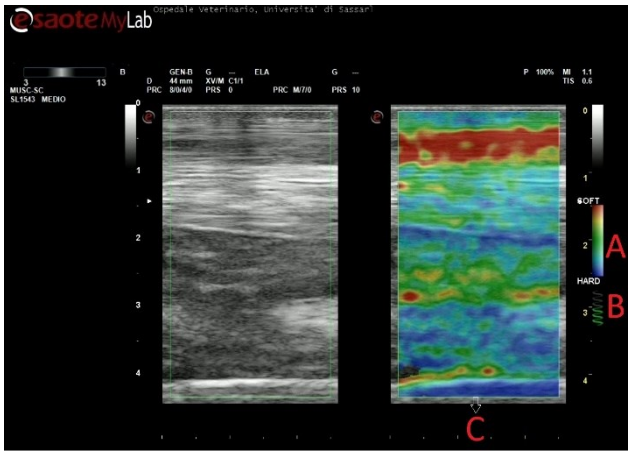

Figure 16. *From Secchi et al (2021). Example of strain elastography. (A) Colour range selected, (B) Indicator for correct compression, (C) Field of view.*

2.4 Image analysis

Twenty images, one of each horse, were randomly selected from the most representative videotapes. Elastograms were considered selectable if they enclosed a SDFT lesion and if the indicator for correct compression was green. The same images were then analysed on the same ultrasound unit by two different veterinarians (VS and AC), who were blinded to each other's results, in order to test inter-observer reproducibility. Image analysis was repeated by one vet (VS) two weeks apart, in order to test intra-observer repeatability.

Image analysis consisted of a measurement of the total area of the SDFT on the longitudinal scan selected and of the area of each predominant colour within the tendon (red, green, and blue). All measurements were performed three times, using the manual tools available on the ultrasound unit, and the mean values were used for further statistical evaluation. Areas were expressed in cm^2.

The same images were then objectively evaluated with ImageJ (Version 1.44)[64].

The evaluation was made on a laptop (Lenovo Ideapad 310-15IKB). Original images (in PNG format), including all the metacarpal structures, were imported into the laptop from the ultrasound unit and cropped along the SDFT perimeter with a basic image editing programme; no other manipulation was performed.

Cropped elastograms showing the injured SDFTs were imported in PNG format and analysed with ImageJ. In each image, the tendon total area and areas of the main colours (red, green and blue) were measured with the "Threshold Color" plugin.

For the selection of colours, the Hue bar was the main tool used, with total hues ranging from 0 (red hues) to 255 (red hues). For the selection of green and blue, a range of hues from 30 to 100 and from 100 to 220 was chosen respectively. On the other hand, the red area was obtained by subtracting green and blue areas from the total areas. Areas were expressed in numbers of pixels (Fig.17).

All the results were recorded in an *ad hoc* database, and the percentage areas of each colour were calculated from the mean values derived from the three consecutive measurements.

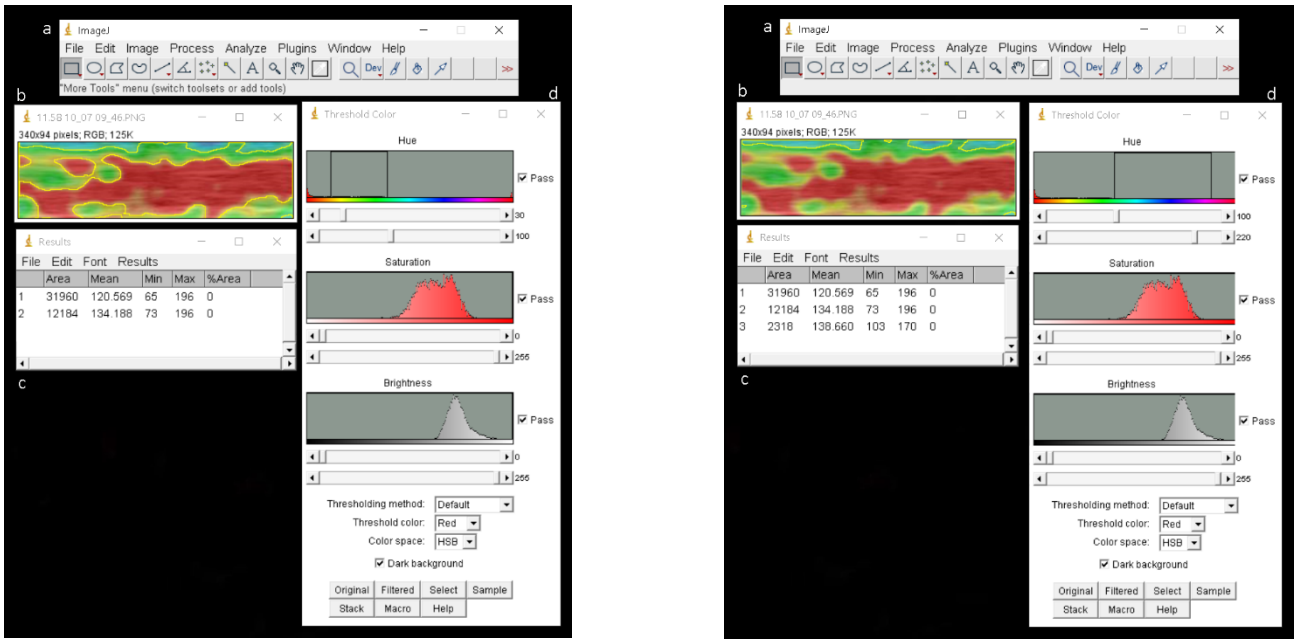

(B) Green selection *(B) Blue selection*

Figure 17. *From Secchi et al (2021). Example of analysis on ImageJ [(a) ImageJ main tool bar, (b) SDFT elastogram image imported, (c) Measurement results, (d) "Threshold color" plugin]. The selection of colours is mainly regulated with the Hue bar, and areas (expressed in pixels) of the selected part are measured.*

2.5 Statistical analysis

The statistical analysis was performed using *R* (Version 3.6.1) [65].

The observed data were triplets $(x_{red}, x_{green}, x_{blue})$ such that $x_{red} + x_{green} + x_{blue} = 100\%$. For example, x_{red} represented the ratio between the red area and the total area of the image, expressed as a percentage. A similar interpretation was given to x_{green} and x_{blue}. Such data structures describe the parts of a whole, and are known in the statistical literature as *compositional data* [66,67]. Mathematically, the observations lie on a 3-part *simplex*, since x_{red}, x_{green} and x_{blue} are constrained to add up to 100%. This constraint violates the assumptions of many standard statistical methods for data analysis. The observations should therefore be projected from the simplex to a 2D real space for further processing. An appropriate transformation is the *isometric log ratio transform* (ILR) [68]. For each observation $(x_{red}, x_{green}, x_{blue})$, the ILR transformation returns a point (y_1, y_2) in the real plane $\mathbb{R}^2$ which is suitable for further statistical analysis:

$$(y_1, y_2) = \mathrm{ILR}(x_{red}, x_{green}, x_{blue}) \quad (1)$$

The ILR-transformed values (y_1, y_2) of the measurements $(x_{red}, x_{green}, x_{blue})$ were used in this work as response variables within the statistical models used for analysis.

A more detailed description of the ILR transform, is given in [68]. Practical details regarding the analysis of compositional data in *R* are given in [69], and the associated package *compositions* [70]. In this work, the default settings of the package were used to calculate the ILR transformation.

Some of the observations for x_{blue} were exactly zero, which must be substituted before applying ILR. We assumed that the zeros arose for percentages of blue below the detection limit of 1%. The zeros were then replaced using a simple rule of two-thirds of the detection limit. A more detailed description of the replacement strategies in compositional data is given in [71].

Since the response variable was bivariate, two-way repeated measures MANOVA was used to assess intra-observer repeatability, grouped by time of measurement and image, restricted to the observations recorded by the veterinarian (VS). The different images were considered as a random effect, and the resulting mixed model was fitted using the package *lme4* [72]. The model assumptions were tested using standard

statistical tests for multivariate observations: normality was tested using Mardia's skewness and kurtosis tests (implemented in *MVN* [73]), and homogeneity of the covariance matrices was tested using Box's M-test (implemented in *heplots* [74]). The models with and without effects for the time of measurement were fitted via maximum likelihood, and the likelihood ratio test was used to assess the difference between them. The adjusted intraclass correlation coefficient (ICC, [75]) was also calculated, with confidence intervals estimated via bootstrapping.

In order to further strengthen the results, intra-observer repeatability was assessed using a one-sample Hotelling's T^2-test (implemented in *ICSNP* [76]), applied on the difference between the two measurements of VS. The Mahalanobis distance calculated for the T^2-test was used as a measure of effect size. Bland-Altman plots [77] were also used to visually assess the agreement between the two measurements, separately for each dimension after the ILR transformation. In order to provide an intuitive interpretation of the results, the boxplots of the differences between the two measurements were also plotted for each of the three colour channels.

Similarly, two-way mixed effects MANOVA was used to evaluate inter-observer repeatability, with grouping factors represented by the veterinarian and the image. The image was considered as random effect, whereas the veterinarian was assumed to be a fixed effect. Model assumptions were tested using the same procedures used for the study on intra-observer repeatability. The likelihood ratio test was used to assess whether the difference between the measurements of the two veterinarians was statistically significant, and the ICC was calculated with bootstrapped confidence intervals. Bland-Altman plots were constructed from an average of the two measurements of VS, compared to the results obtained by AC. Boxplots for the three colour channels were used to provide an intuitive interpretation of the results.

Finally, the difference between the methodologies (manual and ImageJ) was tested using two-way mixed effects MANOVA, fitted on the entire dataset using maximum likelihood, assuming methodology as the fixed effect, and image as the random effect. The underlying model assumptions were again tested using the same procedures described for the two previous studies. The difference between the two methodologies was tested using the likelihood ratio test, which tested the significance of the model coefficients associated

with the manual method and ImageJ. In addition, Bland-Altman plots were used to visually assess the agreement between the two methodologies; the plots were constructed from an average of the three measurements from the manual method, compared to the single measurement obtained from ImageJ. As before, boxplots of the three colour channels were also used to visually assess the difference between the two methodologies. The threshold for significance of the results of each statistical test was assumed to be $\alpha = 0.05$. The criteria of [78] were used to evaluate the ICC: *poor*, (0,0.50); *moderate*, (0.5, 0.75); *good*, (0.75, 0.9); *excellent*, (0.9,1).

3. Results

Figure 18 shows the scatterplots of the measurements before and after the ILR transformation. Table 1 reports the summary statistics of the ILR-transformed data, and Table 2, the corresponding tests for validation of the MANOVA assumptions. The Mardia and Box's *M*-test showed no statistical evidence of violations of any of the model assumptions. The mean and confidence interval for the mean of each of the two dimensions (y_1, y_2) suggested that the two measurements of VS were in agreement, whereas, as expected, more substantial differences were observed in the measurements taken by the different observers (VS and AC) and in the methods (manual and ImageJ).

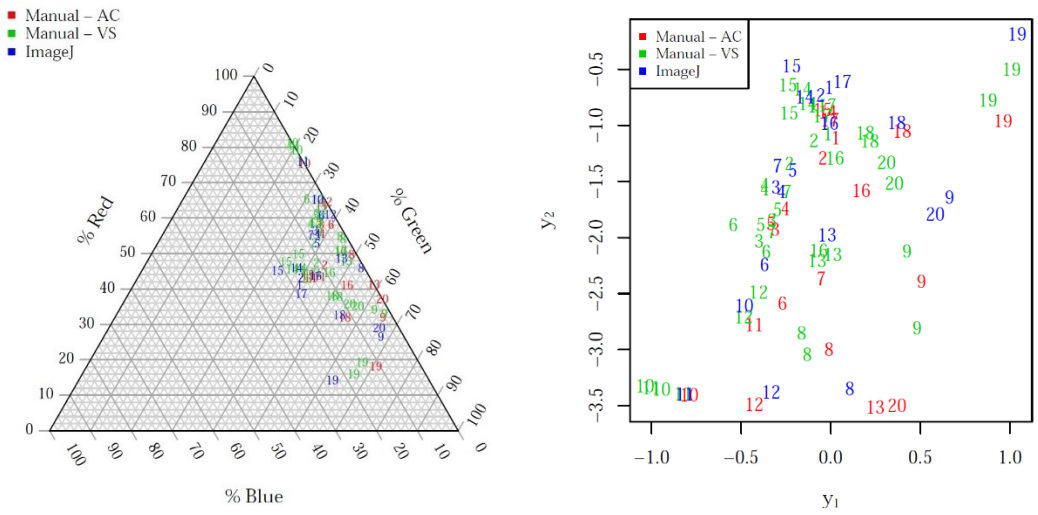

*(**a**) Before ILR transformation* *(**b**) After ILR transformation*

Figure 18. *From Secchi et al (2021). Scatterplot of the measurements before and after the ILR transformation, labelled by image and coloured by observer and method.*

Table 1. *From Secchi et al (2021). Summary (mean and 95% Student's t confidence interval for the mean) of the ILR-transformed data.*

		y_1 (1st dimension of ILR)		y_2 (2nd dimension of ILR)	
Method	**Observer**	**Mean**	**95% C.I.**	**Mean**	**95% C.I.**
Manual	VS (Measurement 1)	−0.174	(−0.371, 0.023)	−1.812	(−2.195, −1.429)
	VS (Measurement 2)	−0.134	(−0.346, 0.078)	−1.728	(−2.146, −1.309)
	AC	−0.015	(−0.198, 0.168)	−2.062	(−2.519, −1.606)
ImageJ	VS	−0.037	(−0.238, 0.164)	−1.582	(−2.044, −1.120)

Table 2. *From Secchi et al (2021). Statistical tests for validation of the mixed effects model assumptions.*

		Mardia's *p*-values		Box's *M p*-value
Method	**Observer**	**Skewness**	**Kurtosis**	**(∼grouping)**
Manual	VS (Measurement 1)	0.314	0.559	0.940 (∼measurement)
	VS (Measurement 2)	0.246	0.538	
	AC	0.615	0.546	0.429 (∼observer)
ImageJ	VS	0.299	0.711	0.957 (∼method)

Intra-observer repeatability, inter-observer reproducibility, and the difference between the manual method and ImageJ were more precisely quantified by the likelihood ratio tests reported in Table 3. The two measurements by VS on the same images did not significantly differ (*p*-value 0.157), demonstrating the intra-observer repeatability of the methodology. This was confirmed by Hotelling's T^2-test on the differences between the measurements on individual images (*p*-value 0.097). The ICC further demonstrated that most of the variability was explained by the differences between the images (adjusted ICC 0.949, with the lower bound of the 95% confidence interval exceeding 0.9), showing excellent intra-observer repeatability. The agreement between the two measurements is also confirmed by Figure 19, which shows the Bland-Altman

plots on each of the two dimensions of the ILR-transformed data, and the boxplot of the difference between the measurements for each colour channel. In the Bland-Altman plots, the observations do not significantly deviate from the horizontal line at zero. In addition, in the boxplots, the differences for each colour channel appear to have a symmetric distribution around zero, further demonstrating the intra-observer repeatability of the methodology.

Table 3. *From Secchi et al (2021). Likelihood ratio test, intraclass correlation coefficient, and Hotelling's T^2-test for the intra-observer repeatability study.*

Likelihood ratio test		**Adjusted ICC**		**Hotelling's T^2-test**	
χ^2 score	*p*-value	Estimate	95% C.I.	Mahalanobis distance	*p*-value
3.698	0.157	0.949	(0.905, 0.972)	2.711	0.094

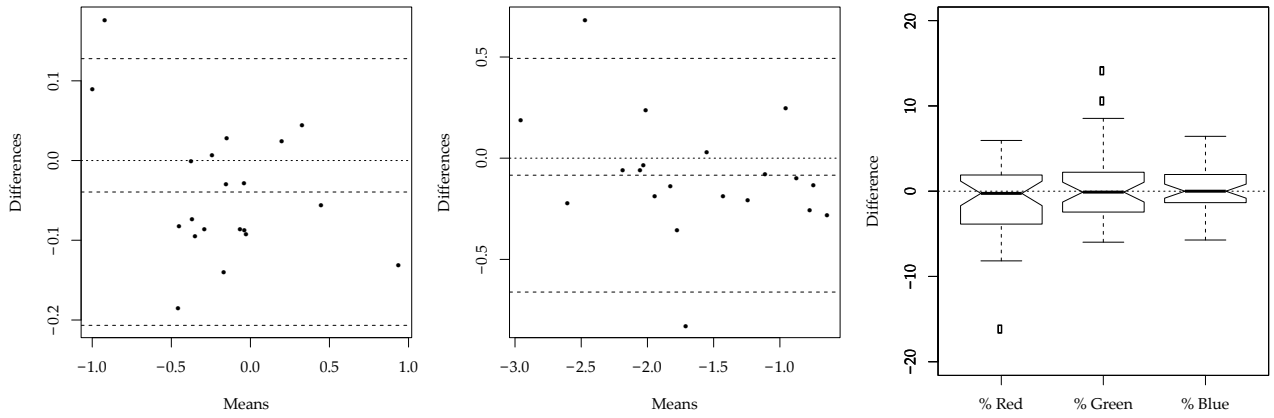

(***a***) *Bland-Altman plot – First dimension of ILR transformed data*

(***b***) *Bland-Altman plot – Second dimension of ILR transformed data*

(***c***) *Boxplots of the differences between the two measurements*

Figure 19. *From Secchi et al (2021). Intra-observer reproducibility study: Bland-Altman plots of the two dimensions of the ILR-transformed data, and boxplot of the difference between the first and second measurement by VS for each colour channel.*

Similar statistical tests were carried out to assess inter-observer reproducibility. From the likelihood ratio test in Table 4, it appeared that the measurements taken by the veterinarians, AC and VS were significantly different (*p*-value <0.001). This is confirmed by Figure 20, as the observations in the Bland-Altman plots are not scattered around the horizontal line at zero, and the boxplots of the differences for the three colour channels are not centred around zero. A significant difference was observed between the two veterinarians in the assessment of the percentages of the colours *red* and *green*. Despite the significant difference between the two observers, the adjusted ICC (0.855, with the lower bound of the 95% confidence interval exceeding 0.75), reported in Table 4 still suggests that there is *good* agreement between the two veterinarians' measurements, since most of the variability is due to the differences *between* the images. The images refer to lesions with different gravity levels and are therefore highly heterogeneous. The variability *between* the measurements on different images is thus much larger than the variability of measurements on the *same* image, which leads to large values of the ICC.

Table 4. *From Secchi et al (2021). Likelihood ratio test and intraclass correlation coefficient for the inter-observer reproducibility study.*

Likelihood ratio test		**Adjusted ICC**	
χ^2 score	*p*-value	Estimate	95% C.I.
18.250	<0.001	0.855	(0.753, 0.907)

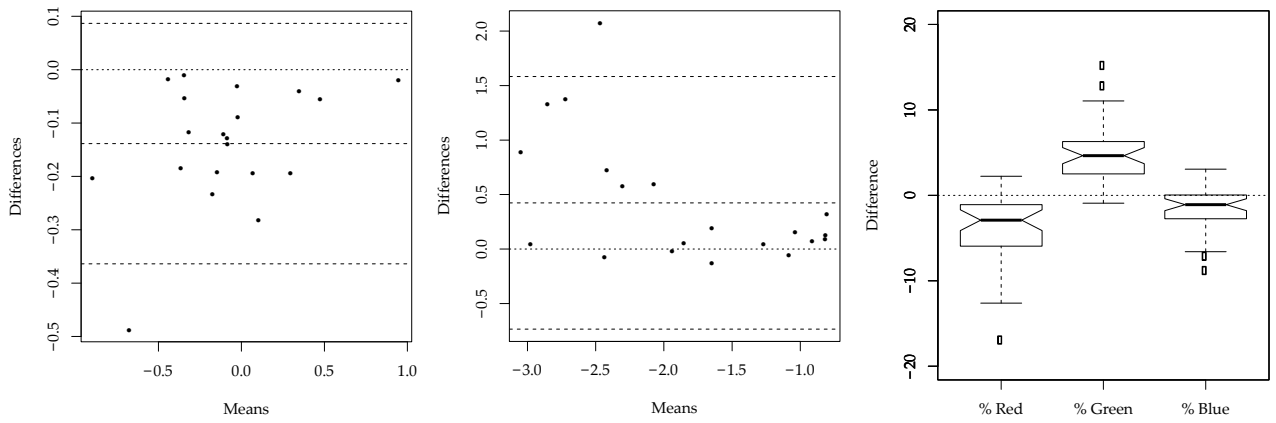

*(**a**) Bland-Altman plot – First dimension of ILR transformed data*

*(**b**) Bland-Altman plot – Second dimension of ILR transformed data*

*(**c**) Boxplots of the differences between the two observers (AC and VS)*

Figure 20. *From Secchi et al (2021). Inter-observer reproducibility study: Bland-Altman plots on the two dimensions of the ILR-transformed data, and boxplot of the difference between the measurements of AC and VS for each colour channel.*

Finally, the difference between the measurements obtained using the manual method and ImageJ was assessed. The likelihood ratio test in Table 5 suggests that there is a statistically significant difference between the measurements obtained using the two methodologies (*p*-value <0.001). Again, this is confirmed by the Bland-Altman plots and boxplots, reported in Figure 21: the observations in the Bland-Altman plots are not randomly distributed around zero, and the boxplots of the differences for the three colour channels show that the measurements of the colours *red* and *blue* significantly deviate from zero. The adjusted ICC (0.849, with the lower bound of the 95% confidence interval exceeding 0.75) in Table 5 demonstrates that, despite the significant differences between the two methodologies, there is a *good* agreement between the measurements. Similarly to the study on inter-observer reproducibility, the ICC is large because most of the variability is due to the differences *between* images.

Table 5. *From Secchi et al (2021). Likelihood ratio test and intraclass correlation coefficient for the study on the differences between the manual method and ImageJ.*

Likelihood ratio test		**Adjusted ICC**	
χ^2 score	*p*-value	Estimate	95% C.I.
16.076	<0.001	0.849	(0.751, 0.899)

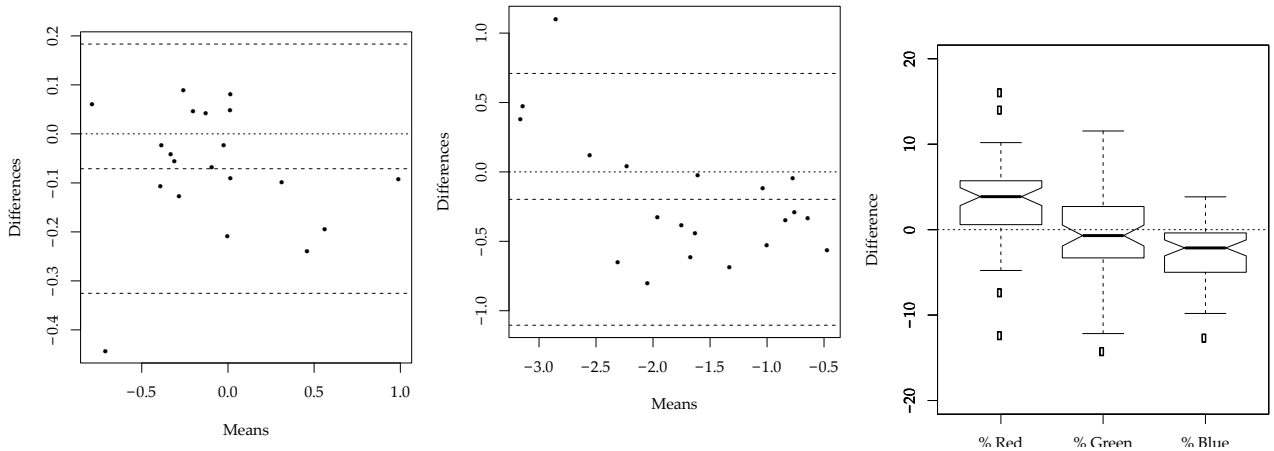

(***a***) *Bland-Altman plot – First dimension of ILR transformed data*

(***b***) *Bland-Altman plot – Second dimension of ILR transformed data*

(***c***) *Boxplots of the differences between the two methods (manual and ImageJ)*

Figure 21. *From Secchi et al (2021). Agreement between manual method and ImageJ: Bland-Altman plots on the two dimensions of the ILR-transformed data, and boxplot of the difference between the measurements obtained using manual method and ImageJ, for each colour channel.*

4. Discussion

The manual measurements of colours in the elastograms of acutely injured SDFTs in horses, showed an *excellent* intra-observer repeatability (ICC 0.949) and a *good* inter-observer reproducibility (ICC 0.855). A *good* agreement was also obtained between the manual method and the ImageJ methodologies of the colour area measurements (ICC 0.849).

The manual measurement of elastograms was thus shown to be a repeatable and reproducible method which could be considered as interchangeable with the objective measurement obtained with the software image analysis.

Our results confirmed previous findings showing that SE image analysis had an almost perfect inter-observer agreement when imaging injured tendons [57]. Moreover, our results showed higher level of agreements compared to a previous study conducted on healthy tendons, in which the qualitative evaluation had moderate inter-observer agreement and good intra-observer agreement [60]. Only one study reported a variability associated both with acquiring and analysing images, which was reported as low [60]. To the best of our knowledge, in equine medicine, no study has reported the standardization of the manual analysis of SE-derived elastograms using image analysis software.

Strain elastography is a qualitative USE technique and is performed by applying a gentle manual rhythmic compression on tissues. It does not produce numerical elasticity parameters, but a relative representation of the elasticity of tissues within the selected window. It is highly operator-dependent, requiring well trained sonographers. In addition accurate acquisitions involve careful preparation [9,10,23,79,80].

Healthy equine SDFTs normally appear in elastograms as predominantly blue structures, with a mostly green peritendinous tissue, and surrounded by soft tissue structures, which appear as red [60]. When a lesion occurs, during the acute inflammatory phase, the injured area of the tendons becomes softer (red), due to haemorrhage, oedema, and fibrin clot organization [81]. As the granulation tissue forms, tendons become more stable, and the colour changes to yellow/green, representing intermediate stiffness [82,83]. During the remodelling phase, tendons become progressively harder, returning to their original mechanical properties (mainly blue) [84].

In order to obtain accurate elastograms of SDFTs in horses, animals should be evaluated under weight-bearing conditions, because there are usually fewer artefacts in the elastographic evaluation compared to a non-weight-bearing position [57,60]. Minimal precompression should be used in order to prevent precompression artefacts. In fact, when excessive precompression is exerted, elastograms are not representative of the real mechanical characteristics of tissues [23]. The visual indicator for correct compression does not consider the precompression degree, and thus could appear green despite an insufficiently accurate evaluation. In our study, elastographic examinations of the SDFT were relatively easy to perform, due to the superficial location of the examined structure, thus obtaining a qualitative representation of the mechanical properties of pathologic tendons. We only analysed longitudinal images due to problems encountered in obtaining elastograms in the short-axis view, especially in distal levels of the metacarpus. Images of transverse planes showed more artefacts than longitudinal ones, especially on medial and lateral parts, due to the convex margins of the tendons. Both in human medicine, for the evaluation of Achilles tendons, and in veterinary medicine, for the evaluation of SDFTs in horses, and calcaneal and patellar tendons in dogs, longitudinal images are preferred because they are considered to be of a better quality, while transverse images show more artefacts and lower reproducibility [40,54,56,58].

The SE images were obtained without a standoff pad which can be problematic for a correct evaluation of the elasticity pattern. The lack of accurate contact between the probe and standoff pad can produce reverberation artifacts, which are visible as parallel red areas in the elastogram, which can be confused with areas of softness [59,60]. In addition, the inclusion of the pad in the Fov can alter the colour pattern of SE-derived elastograms, because of its well-known relativity. The standoff pad can represent the softest part within the elastographic window, and as a consequence, SDFT lesions can be misinterpreted or underestimated, no longer appearing as red but yellow/green, in other words with an intermediate stiffness. Finally, the use of the pad can alter the elasticity estimation since the deepest structures, which we decided to include (suspensory ligament and cannon bone), are probably more difficult to reach. This can subsequently lead to a lack of signal, without any colour (Fig. 22).

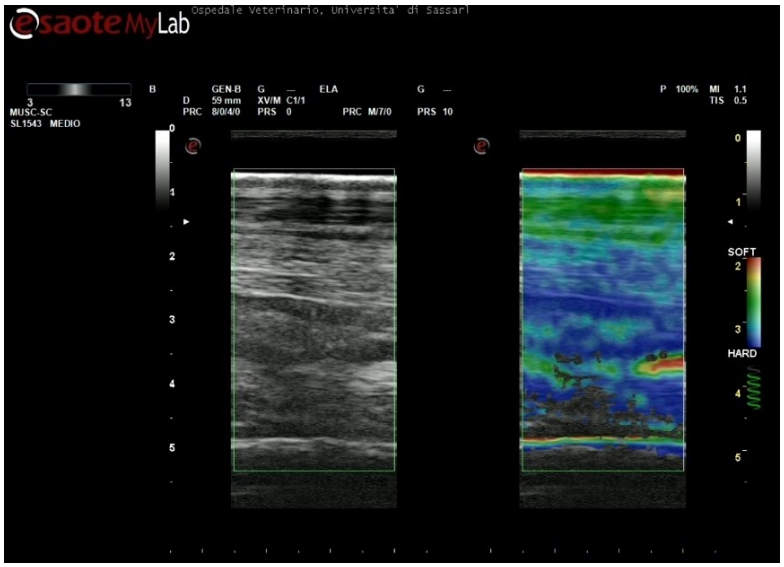

Figure 22. *From Secchi et al (2021). At the bottom of the Fov, an artifact is present as a lack of signal, without any colours. This could be explained by the use of the pad as the deepest structures, where the artifact appears, are probably more difficult to reach, compared with images obtained without pad. Secondly, the inclusion of a standoff pad within Fov can alter the colour pattern of SE-derived elastograms, because of its relativity; the standoff pad can represent the softest part within elastographic window, and as s consequence, the SDFT lesions can be misinterpreted or underestimated, no longer appearing red but yellow/green.*

In our trials, it was not necessary to sedate the horses, however the use of a sedative is recommended if needed. The influence of sedation on USE results is still controversial, with some authors stating that the results are not compromised [58,60] and others declaring that images can be potentially influenced by sedation[85].

For the SE image analysis, categorical colour-grading is normally the most common system used. It is a qualitative method which was first used in human medicine for the evaluation of Achilles tendons [27,86] and subsequently adapted for equine SDFTs [57,60]. This simple categorical assessment facilitates a semi-quantitative analysis of data, with high interobserver agreement and applicability in clinical practice[57,58].

However, due the subjective nature of colour-grading, we used ImageJ for a more objective analysis, which we compared with a manual assessment using an ultrasound unit. As recommended [87,88], the evaluation consisted in calculating the percentage of the three main colours present in the elastograms: red (softest structures), green (intermediate stiffness), and blue (stiffest areas).

The software analysis was performed with the “Threshold color” plugin, because it was considered easier to interpret clinically and more reproducible than qualitative or quantitative methods, which measure the mean echo-intensity for each colour considered [87,89,90].

A significant difference was initially observed between the two veterinarians’ (VS and AC) measurements and the measurements taken using the two methodologies However, the subsequent analyses established that most of the variability was due to differences between images, thus in reality good ICCs were obtained.

Differences between images could be explained considering different sizes, distributions and shapes of the coloured areas which characterize injured tendon elastograms. For example, measuring an area with a regular and bigger shape is simpler than measuring an area with an irregular and smaller shape. This can be explained clinically by the heterogeneity of the SDFT lesions included in the sample. As a consequence, some elastograms were very different than others, in terms of the proportion, morphology, and margins of colours within Fov.

Moreover, the differences in tracing could also be a product of the differences in the visual perception of colours, caused by the wide range of hues in the elastograms. Different shapes and irregular distributions of colours could also make the visual perception problematic.

The study has several limitations.

Firstly, a small sample size was recruited with a relative heterogeneity regarding the region and gravity of disease. However, patients were homogenous concerning breed, activity, and the time of diagnosis from the injury onset.

Secondly, two-dimensional ultrasonography and SE are both considered highly operator dependent methods and, especially for SE, several precautions had to be taken, as previously explained. For this reason, all the evaluations were performed by the same trained veterinarian (VS). In addition, strain elastography is a type of USE that shows a relative categorization of tissue elasticity. Other methods, such as SWE, which provide objective numerical parameters, could be more reliable, and the data obtained may be easier to analyse. Moreover, USE is still not commonly used in veterinary medicine, thus more studies and

comparisons are needed in order to standardize the method and subsequent analysis. However, this is still difficult due to the high variability of procedures and analysis techniques present in the literature.

No histopathologic assessment was performed, since all cases consisted of racehorses undergoing rehabilitation in order to return to competition.

Finally, image analysis using ImageJ was a long and complex procedure and several parameters needed to be considered. Despite the easy automatic selection and measurement of coloured areas by the software, ranges of hue, saturation, and brightness (Fig.1) had to be previously selected and tested by the operator, since a minimal change in range selection of each parameter can influence the results. To prove this, an evaluation was performed, considering different configurations of hue, brightness, and saturation, showing significant differences between images categorizations. For this reason, a standardization of the selection of ranges is needed in order to make the assessment as accurate as possible, which should correspond as much as possible to the manual assessment. Furthermore, the low use of ImageJ and especially of “Threshold color” plugin in veterinary medicine provided few models for comparison.

5. Conclusions

This study demonstrates that the manual measurements of colours within elastograms of pathologic tendons showed a good and excellent inter- and intra-observer reliability, respectively.

In addition, a good agreement was also obtained between the manual and ImageJ analyses, for the evaluation of injured SDFTs in horses. We believe that this demonstrates that manual measurement is a feasible and accurate method, and that it could be considered as valid as the objective software assessment. As an accurate interpretation and measurement of lesions is fundamental, it could thus be used to evaluate tendon healing.

Future studies are recommended to better evaluate the potential of SE for musculo-skeletal structures and different imaging analysis techniques in horses.

6. Bibliography

1. Goodship, A. E., Birch, H. L. & Wilson, A. M. The pathobiology and repair of tendon and ligament injury. *Vet. Clin. North Am. Equine Pract.* **10**, 323–349 (1994).

2. Liu, Y., Ramanath, H. S. & Wang, D. A. Tendon tissue engineering using scaffold enhancing strategies. *Trends Biotechnol.* **26**, 201–209 (2008).

3. Franchi, M., Trirè, A., Quaranta, M., Orsini, E. & Ottani, V. Collagen structure of tendon relates to function. *ScientificWorldJournal.* **7**, 404–420 (2007).

4. Barfod, K. W. Achilles tendon rupture; Assessment of non- operative treatment Achilles tendon Total Rupture Score Standard Error of the Measurement. *Dan. Med. J.* **61**, 1–26 (2014).

5. Biewener, A. A. Muscle-tendon stresses and elastic energy storage during locomotion in the horse. *Comp. Biochem. Physiol. B. Biochem. Mol. Biol.* **120**, 73–87 (1998).

6. Riemersma, D. J. & Schamhardt, H. C. In vitro mechanical properties of equine tendons in relation to cross-sectional area and collagen content. *Res. Vet. Sci.* **39**, 263–270 (1985).

7. Patterson-Kane, J. C., Wilson, A. M., Firth, E. C., Parry, D. A. D. & Goodship, A. E. Comparison of collagen fibril populations in the superficial digital flexor tendons of exercised and nonexercised Thoroughbreds. *Equine Vet. J.* **29**, 121–125 (1997).

8. Bleakney, R. R. & White, L. M. Imaging of the Achilles Tendon. *Foot Ankle Clin.* **10**, 239–254 (2005).

9. Ooi, C. C., Malliaras, P., Schneider, M. E. & Connell, D. A. 'Soft, hard, or just right?' Applications and limitations of axial-strain sonoelastography and shear-wave elastography in the assessment of tendon injuries. *Skeletal Radiol.* **43**, 1–12 (2014).

10. Klauser, A., Faschingbauer, R. & Jaschke, W. Is Sonoelastography of Value in Assessing Tendons? *Semin. Musculoskelet. Radiol.* **14**, 323–333 (2010).

11. Möller, M. *et al.* The ultrasonographic appearance of the ruptured Achilles tendon during healing: a

longitudinal evaluation of surgical and nonsurgical treatment, with comparisons to MRI appearance. *Knee Surgery, Sport. Traumatol. Arthrosc. 2001 101* **10**, 49–56 (2001).

12. Khan, K. M. *et al.* Are ultrasound and magnetic resonance imaging of value in assessment of Achilles tendon disorders? A two year prospective study. *Br. J. Sports Med.* **37**, 149–153 (2003).

13. Smith, R. K. W. & Cauvin, E. R. J. Ultrasonography of the Metacarpus and Metatarsus. in *Atlas of Equine Ultrasonography* (eds. Kidd, J. A., Lu, K. G. & Frazer, M. L.) 73–105 (John Wiley & Sons, Ltd, 2014).

14. Ophir, J., Céspedes, I., Ponnekanti, H., Yazdi, Y. & Li, X. Elastography: A quantitative method for imaging the elasticity of biological tissues. *Ultrason. Imaging* **13**, 111–134 (1991).

15. Garra, B. Elastography: current status, future prospects, and making it work for you. *Ultrasound Q.* **27**, 177–186 (2011).

16. Garra, B. Imaging and estimation of tissue elasticity by ultrasound. *Ultrasound Q.* **23**, 255–268 (2007).

17. Hall, T. AAPM/RSNA physics tutorial for residents: topics in US: beyond the basics: elasticity imaging with US. *Radiographics* **23**, 1657–1671 (2003).

18. Lerner, R., SR, H. & KJ, P. 'Sonoelasticity' images derived from ultrasound signals in mechanically vibrated tissues. *Ultrasound Med. Biol.* **16**, 231–239 (1990).

19. Bojunga, J. *et al.* Acoustic Radiation Force Impulse Imaging for Differentiation of Thyroid Nodules. *PLoS One* **7**, e42735 (2012).

20. Wick, M. C. & Jaschke, W. R. Sonoelastography : Musculoskeletal. **272**, (2014).

21. Winn, N., Lalam, R. & Cassar-Pullicino, V. Sonoelastography in the musculoskeletal system: Current role and future directions. *World J. Radiol.* **8**, 868 (2016).

22. Prado-Costa, R., Rebelo, J., Monteiro-Barroso, J. & Preto, A. S. Ultrasound elastography:

compression elastography and shear-wave elastography in the assessment of tendon injury. *Insights Imaging* 1–24 (2018) doi:10.1007/s13244-018-0642-1.

23. Barr, R. G. Strain elastography. in *Breast Elastography* 11–30 (Thieme Medical Publishers, Inc., 2015). doi:10.1177/1742271x15618181.

24. Vlad, M. *et al.* Real-time shear wave elastography may predict autoimmune thyroid disease. *Wien. Klin. Wochenschr.* **127**, 330–336 (2015).

25. Bouillard, K., Nordez, A. & Hug, F. Estimation of Individual Muscle Force Using Elastography. *PLoS One* **6**, e29261 (2011).

26. De Zordo, T. *et al.* Real-time sonoelastography: Findings in patients with symptomatic achilles tendons and comparison to healthy volunteers. *Ultraschall der Medizin* **31**, 394–400 (2010).

27. De Zordo, T. *et al.* Real-time sonoelastography findings in healthy Achilles tendons. *Am. J. Roentgenol.* **193**, (2009).

28. Drakonaki, E. E., Allen, G. M. & Wilson, D. J. Ultrasound elastography for musculoskeletal applications. *British Journal of Radiology* vol. 85 1435–1445 (2012).

29. Sconfienza, L. M., Orlandi, D., Cimmino, M. A. & Silvestri, E. A Few Considerations on "Sonoelastography of the Plantar Fascia". *Radiology* **261**, 995–996 (2011).

30. Park, G. & DR, K. Application of real-time sonoelastography in musculoskeletal diseases related to physical medicine and rehabilitation. *Am. J. Phys. Med. Rehabil.* **90**, 875–886 (2011).

31. De Zordo, T. *et al.* Real-time sonoelastography of lateral epicondylitis: Comparison of findings between patients and healthy volunteers. *Am. J. Roentgenol.* **193**, 180–185 (2009).

32. Schwab, F. *et al.* Inter- and Intra-observer Agreement in Ultrasound BI-RADS Classification and Real-Time Elastography Tsukuba Score Assessment of Breast Lesions. (2016) doi:10.1016/j.ultrasmedbio.2016.06.017.

33. Choi, Y. J., Lee, J. H. & Baek, J. H. Ultrasound elastography for evaluation of cervical lymph nodes. *Ultrasonography* **34**, 157–164 (2015).

34. Itoh, A. *et al.* Breast Disease: Clinical Application of US Elastography for Diagnosis. *Radiology* **239**, 341–350 (2006).

35. Rubaltelli, L. *et al.* Differential diagnosis of benign and malignant thyroid nodules at elastosonography. *Ultraschall der Medizin* **30**, 175–179 (2009).

36. Pallwein, L. *et al.* Comparison of sonoelastography guided biopsy with systematic biopsy: Impact on prostate cancer detection. *Eur. Radiol.* **17**, 2278–2285 (2007).

37. Ophir, J. *et al.* Elastography: Ultrasonic estimation and imaging of the elastic properties of tissues. *Proc. Inst. Mech. Eng. Part H J. Eng. Med.* **213**, 203–233 (1999).

38. Manzoor, I., Bacha, R. & Gilani, S. A. Diagnostic accuracy of sonoelastography in different diseases. *J. Ultrason.* **18**, 29–36 (2018).

39. Domenichini, R., Pialat, J. B., Podda, A. & Aubry, S. Ultrasound elastography in tendon pathology: state of the art. *Skeletal Radiol.* **46**, 1643–1655 (2017).

40. Drakonaki, E. E., Allen, G. M. & Wilson, D. J. Real-time ultrasound elastography of the normal Achilles tendon: reproducibility and pattern description. *Clin. Radiol.* **64**, 1196–1202 (2009).

41. Silvestri, E., Minetti, G., Schettini, D., D'Auria, M. C. & Cimmino, M. A. Sonoelastography can help in the localization of soft tissue damage in polymyalgia rheumatica (PMR) [7]. *Clin. Exp. Rheumatol.* **25**, 796 (2007).

42. Sconfienza, L. M., Silvestri, E., Bartolini, B., Garlaschi, G. & Cimmino, M. A. Sonoelastography may help in the differential diagnosis between rheumatoid nodules and tophi. *Clin. Exp. Rheumatol.* **28**, 144–145 (2010).

43. Wu, C., Chang, K., Mio, S., Chen, W. & Wang, T. Sonoelastography of the Plantar Fascia. **259**, (2011).

44. Lee, G. *et al.* STRAIN ELASTOGRAPHY USING DOBUTAMINE-INDUCED CAROTID ARTERY PULSATION IN CANINE THYROID GLAND. *Vet. Radiol. Ultrasound* **56**, 549–553 (2015).

45. Alder, D., Bass, D., Spörri, M., Kircher, P. & Ohlerth, S. Does real-time elastography aid in differentiating canine splenic nodules? *Schweiz. Arch. Tierheilkd.* **155**, 491–496 (2013).

46. Seiler, G. S. & Griffith, E. Comparisons between elastographic stiffness scores for benign versus malignant lymph nodes in dogs and cats. *Vet. Radiol. Ultrasound* **59**, 79–88 (2018).

47. Choi, M., Yoon, J. & Choi, M. Contrast-enhanced ultrasound sonography combined with strain elastography to evaluate mandibular lymph nodes in clinically healthy dogs and those with head and neck tumors. *Vet. J.* **257**, 105447 (2020).

48. Domosławska, A., Zduńczyk, S., Jurczak, A. & Janowski, T. Elastography as a diagnostic tool in the prostate tumour detection in Labrador retriever. *Andrologia* **50**, (2018).

49. Cintra, C. A. *et al.* Applicability of ARFI Elastography in the Evaluation of Canine Prostatic Alterations Detected by b-mode and Doppler Ultrasonography. *Arq. Bras. Med. Vet. e Zootec.* **72**, 2135–2140 (2020).

50. Feliciano, M. A. R. *et al.* ARFI elastography as a complementary diagnostic method for mammary neoplasia in female dogs - preliminary results. *J. Small Anim. Pract.* **55**, 504–508 (2014).

51. Feliciano, M. A. R. *et al.* Accuracy of four ultrasonography techniques in predicting histopathological classification of canine mammary carcinomas. *Vet. Radiol. Ultrasound* **59**, 444–452 (2018).

52. Longo, M., Bavcar, S., Handel, I., Smith, S. & Liuti, T. Real-time elastosonography of lipomatous vs. malignant subcutaneous neoplasms in dogs: Preliminary results. *Vet. Radiol. Ultrasound* **59**, 198–202 (2018).

53. Glińska-Suchocka, K. *et al.* Application of shear wave elastography in the diagnosis of mammary gland neoplasm in dogs. *Pol. J. Vet. Sci.* **16**, 477–482 (2013).

54. Del Signore, F. *et al.* Sonoelastography of Normal Canine Common Calcaneal Tendon: Preliminary Results. *Vet. Comp. Orthop. Traumatol.* (2020) doi:10.1055/s-0040-1721660.

55. Ellison, M. *et al.* Feasibility and repeatability for in vivo measurements of stiffness gradients in the canine gastrocnemius tendon using an acoustoelastic strain gauge. *Vet. Radiol. Ultrasound* **54**, 548–554 (2013).

56. Piccionello, A. P. *et al.* Sonoelastographic Features of the Patellar Ligament in Clinically Normal Dogs. *Vet. Comp. Orthop. Traumatol.* **31**, 279–284 (2018).

57. Tamura, N. *et al.* Application of sonoelastography for evaluating the stiffness of equine superficial digital flexor tendon during healing. *Vet. Rec.* **180**, 120 (2017).

58. Tamura, N. *et al.* The use of sonoelastography to assess the recovery of stiffness after equine superficial digital flexor tendon injuries: A preliminary prospective longitudinal study of the healing process. *Equine Vet. J.* **49**, 590–595 (2017).

59. Lustgarten, M. *et al.* Elastographic evaluation of naturally occuring tendon and ligament injuries of the equine distal limb. *Vet. Radiol. Ultrasound* **56**, 670–679 (2015).

60. Lustgarten, M. *et al.* Elastographic characteristics of the metacarpal tendons in horses without clinical evidence of tendon injury. *Vet. Radiol. Ultrasound* **55**, 92–101 (2014).

61. Ellison, M. E., Duenwald-kuehl, S., Forrest, L. J., Jr, R. V. & Brounts, S. H. Reproducibility and feasibility of acoustoelastography in the superficial digital flexor tendons of clinically normal horses.

62. Crevier-Denoix, N., Ravary-Plumioën, B., Evrard, D. & Pourcelot, P. Reproducibility of a non-invasive ultrasonic technique of tendon force measurement, determined in vitro in equine superficial digital flexor tendons. *J. Biomech.* **42**, 2210–2213 (2009).

63. Palgrave, K. & Kidd, J. A. Introduction. in *Atlas of Equine Ultrasonography* (eds. Kidd, J. A., Lu, K. G. & Frazer, M. L.) 1–22 (John Wiley & Sons, Ltd, 2014). doi:10.1111/j.1751-0813.1999.tb11242.x.

64. Schneider, C. A., Rasband, W. S. & Eliceiri, K. W. NIH Image to ImageJ: 25 years of image analysis. *Nature Methods* vol. 9 671–675 (2012).

65. R Core Team. *R: A Language and Environment for Statistical Computing*. (2019).

66. Aitchison, J. The Statistical Analysis of Compositional Data. *J. R. Stat. Soc. Ser. B* **44**, 139–177 (1982).

67. Aitchison, J. *The Statistical Analysis of Compositional Data*. (Chapman & Hall, Ltd., 1986).

68. Egozcue, J. J., Pawlowsky-Glahn, V., Mateu-Figueras, G. & Barceló-Vidal, C. Isometric Logratio Transformations for Compositional Data Analysis. *Math. Geol.* **35**, 279–300 (2003).

69. van den Boogaart, K. G. & Tolosana-Delgado, R. *Analyzing Compositional Data with R*. (Springer, 2013).

70. van den Boogaart, K. G., Tolosana-Delgado, R. & Bren, M. compositions: Compositional Data Analysis. (2020).

71. Martin-Fernández, J. A., Barceló-Vidal, C. & Pawlowsky-Glahn, V. Dealing with Zeros and Missing Values in Compositional Data Sets Using Nonparametric Imputation. *Math. Geol.* **35**, 253–278 (2003).

72. Bates, D., Mächler, M., Bolker, B. & Walker, S. Fitting Linear Mixed-Effects Models Using {lme4}. *J. Stat. Softw.* **67**, 1–48 (2015).

73. Korkmaz, S., Goksuluk, D. & Zararsiz, G. MVN: An R Package for Assessing Multivariate Normality. *R J.* **6**, 151–162 (2014).

74. Fox, J., Friendly, M. & Monette, G. heplots: Visualizing Tests in Multivariate Linear Models. R package version 1.3-8. (2020).

75. Nakagawa, S., Johnson, P. C. D. & Schielzeth, H. The coefficient of determination R2 and intra-class correlation coefficient from generalized linear mixed-effects models revisited and expanded. *J. R. Soc. Interface* **14**, (2017).

76. Nordhausen, K., Sirkia, S., Oja, H. & Tyler, D. E. ICSNP: Tools for Multivariate Nonparametrics. (2018).

77. Bland, J. M. & Altman, D. G. Statistical methods for assessing agreement between two methods of clinical measurement. *Lancet* **1**, 307–310 (1986).

78. Koo, T. K. & Li, M. Y. A Guideline of Selecting and Reporting Intraclass Correlation Coefficients for Reliability Research. *J. Chiropr. Med.* **15**, 155–163 (2016).

79. Prado-Costa, R., Rebelo, J., Monteiro-Barroso, J. & Preto, A. S. Ultrasound elastography: compression elastography and shear-wave elastography in the assessment of tendon injury. *Insights Imaging* **9**, 791–814 (2018).

80. Fusini, F. *et al.* Real-time sonoelastography: Principles and clinical applications in tendon disorders. a systematic review. *Muscles. Ligaments Tendons J.* **7**, 467–477 (2017).

81. Patterson-Kane, J. C. & Firth, E. C. The pathobiology of exercise-induced superficial digital flexor tendon injury in Thoroughbred racehorses. *Vet. J.* **181**, 79–89 (2009).

82. Williams, I. F., Heaton, A. & McCullagh, K. G. Cell morphology and collagen types in equine tendon scar. *Res. Vet. Sci.* **28**, 302–310 (1980).

83. Cheung, D. T., DiCesare, P., Benya, P. D., Libaw, E. & Nimni, M. E. The presence of intermolecular disulfide cross-links in type III collagen. *J. Biol. Chem.* **258**, 7774–7778 (1983).

84. Sharma, P. & Maffulli, N. Tendon injury and tendinopathy: Healing and repair. *Journal of Bone and Joint Surgery - Series A* vol. 87 187–202 (2005).

85. De Gasperi, D., Dzierzak, S. L., Muir, P., Vanderby, R. & Brounts, S. H. In vivo evaluation of effects of sedation on results of acoustoelastography of the superficial digital flexor tendons in clinically normal horses. *Am. J. Vet. Res.* **78**, 1421–1425 (2017).

86. Klauser, A. S. *et al.* Achilles tendon assessed with sonoelastography: Histologic agreement. *Radiology* **267**, 837–842 (2013).

87. Martínez-Payá, J. J., del Baño-Aledo, M. E., Ríos-Díaz, J., Fornés-Ferrer, V. & Vázquez-Costa, J. F. Sonoelastography for the Assessment of Muscle Changes in Amyotrophic Lateral Sclerosis: Results of a Pilot Study. *Ultrasound Med. Biol.* **44**, 2540–2547 (2018).

88. Teng, P. P. C. & Lo, Y. L. A Comparison Study of Conventional Ultrasound and Ultrasound Strain Elastography in the Evaluation of Myopathy. *Ultrasound Q.* **36**, 32–37 (2020).

89. Ríos-Díaz, J. *et al.* Sonoelastography of Plantar Fascia: Reproducibility and Pattern Description in Healthy Subjects and Symptomatic Subjects. *Ultrasound Med. Biol.* **41**, 2605–2613 (2015).

90. Magarelli, N. *et al.* Sonoelastography for qualitative and quantitative evaluation of superficial soft tissue lesions: A feasibility study. *Eur. Radiol.* **24**, 566–573 (2014).